AGU PUBLICATIONS

Tectonics

RESEARCH ARTICLE
10.1002/2017TC004498

Key Points:
- Exhumation of the Santa Rosa Mountains (SRM) initiated at circa 8 Ma via low-angle extension along the West Salton Detachment Fault
- Correction of Pleistocene to recent NE tilt of the SRM and thermal modeling improve precision of exhumation initiation timing
- Local fault geometry, not plate motion obliquity, exerts primary control on rock uplift rates in the SRM since circa 1.2 Ma

Supporting Information:
- Supporting Information S1

Correspondence to:
C. C. Mason,
cmason80@vt.edu

Citation:
Mason, C. C., Spotila, J. A., Axen, G., Dorsey, R. J., Luther, A., & Stockli, D. F. (2017). Two-phase exhumation of the Santa Rosa Mountains: Low- and high-angle normal faulting during initiation and evolution of the southern San Andreas Fault system. *Tectonics*, *36*. https://doi.org/10.1002/2017TC004498

Received 1 FEB 2017
Accepted 17 OCT 2017
Accepted article online 26 OCT 2017

Two-Phase Exhumation of the Santa Rosa Mountains: Low- and High-Angle Normal Faulting During Initiation and Evolution of the Southern San Andreas Fault System

Cody C. Mason[1], James A. Spotila[1], Gary Axen[2], Rebecca J. Dorsey[3], Amy Luther[4], and Daniel F. Stockli[5]

[1]Department of Geosciences, Virginia Polytechnic Institute and State University, Blacksburg, VA, USA, [2]Department of Earth and Environmental Science, New Mexico Institute if Mining and Technology, Socorro, NM, USA, [3]Department of Earth Sciences, University of Oregon, Eugene, OR, USA, [4]Department of Geology and Geophysics, Louisiana State University, Baton Rouge, LA, USA, [5]Department of Geological Sciences, University of Texas at Austin, Austin, TX, USA

Abstract Low-angle detachment fault systems are important elements of oblique-divergent plate boundaries, yet the role detachment faulting plays in the development of such boundaries is poorly understood. The West Salton Detachment Fault (WSDF) is a major low-angle normal fault that formed coeval with localization of the Pacific-North America plate boundary in the northern Salton Trough, CA. Apatite U-Th/He thermochronometry (AHe; $n = 29$ samples) and thermal history modeling of samples from the Santa Rosa Mountains (SRM) reveal that initial exhumation along the WSDF began at circa 8 Ma, exhuming footwall material from depths of >2 to 3 km. An uplifted fossil (Miocene) helium partial retention zone is present in the eastern SRM, while a deeper crustal section has been exhumed along the Pleistocene high-angle Santa Rosa Fault (SFR) to much higher elevations in the southwest SRM. Detachment-related vertical exhumation rates in the SRM were ~0.15–0.36 km/Myr, with maximum fault slip rates of ~1.2–3.0 km/Myr. Miocene AHe isochrons across the SRM are consistent with northeast crustal tilting of the SRM block and suggest that the post-WSDF vertical exhumation rate along the SRF was ~1.3 km/Myr. The timing of extension initiation in the Salton Trough suggests that clockwise rotation of relative plate motions that began at 8 Ma is associated with initiation of the southern San Andreas system. Pleistocene regional tectonic reorganization was contemporaneous with an abrupt transition from low- to high-angle faulting and indicates that local fault geometry may at times exert a fundamental control on rock uplift rates along strike-slip fault systems.

Plain Language Summary The southern San Andreas Fault system is an important component of the Pacific-North America plate tectonic boundary, but the age of initiation of this significant geological feature in southern California is disputed. We investigated the uplift history of the Santa Rosa Mountains, west of the San Andreas Fault in Coachella Valley, California, by measuring helium in crystals called apatite. The technique known as thermochronometry lets us learn the cooling history and thus the uplift history of mountain ranges. Our work shows that the Southern San Andreas system began forming with extension of Earth's crust along a low-angle normal fault 8 Ma ago. The timing of southern San Andreas formation was probably synchronous with the beginning of widespread strike-slip faulting in the Baja Mexico area that would later become the Gulf of California. Much later, around 1 Ma ago, a new strike-slip fault, called the San Jacinto Fault, deactivated and cut the low-angle fault and uplifted the southwest Santa Rosa Mountains. This event was associated with punctuated, surprisingly high rates of uplift. These results help geologists to reconstruct the history of this plate boundary and to learn how mountains form along oblique-extensional and strike-slip fault systems.

1. Introduction

Extensional kinematics of transform-related basins may be complex, with phases of extension along both high- and low-angle structures. Low-angle normal faults (dip <30°) are a globally important feature in extensional continental tectonics (Axen, 1999; Wernicke, 1985) and may play an import role in the evolution of oblique-divergent and transform plate boundaries (Axen & Fletcher, 1998). Systems composed of semiparallel low-angle normal faults and strike-slip faults occur in several localities along the Pacific-North America

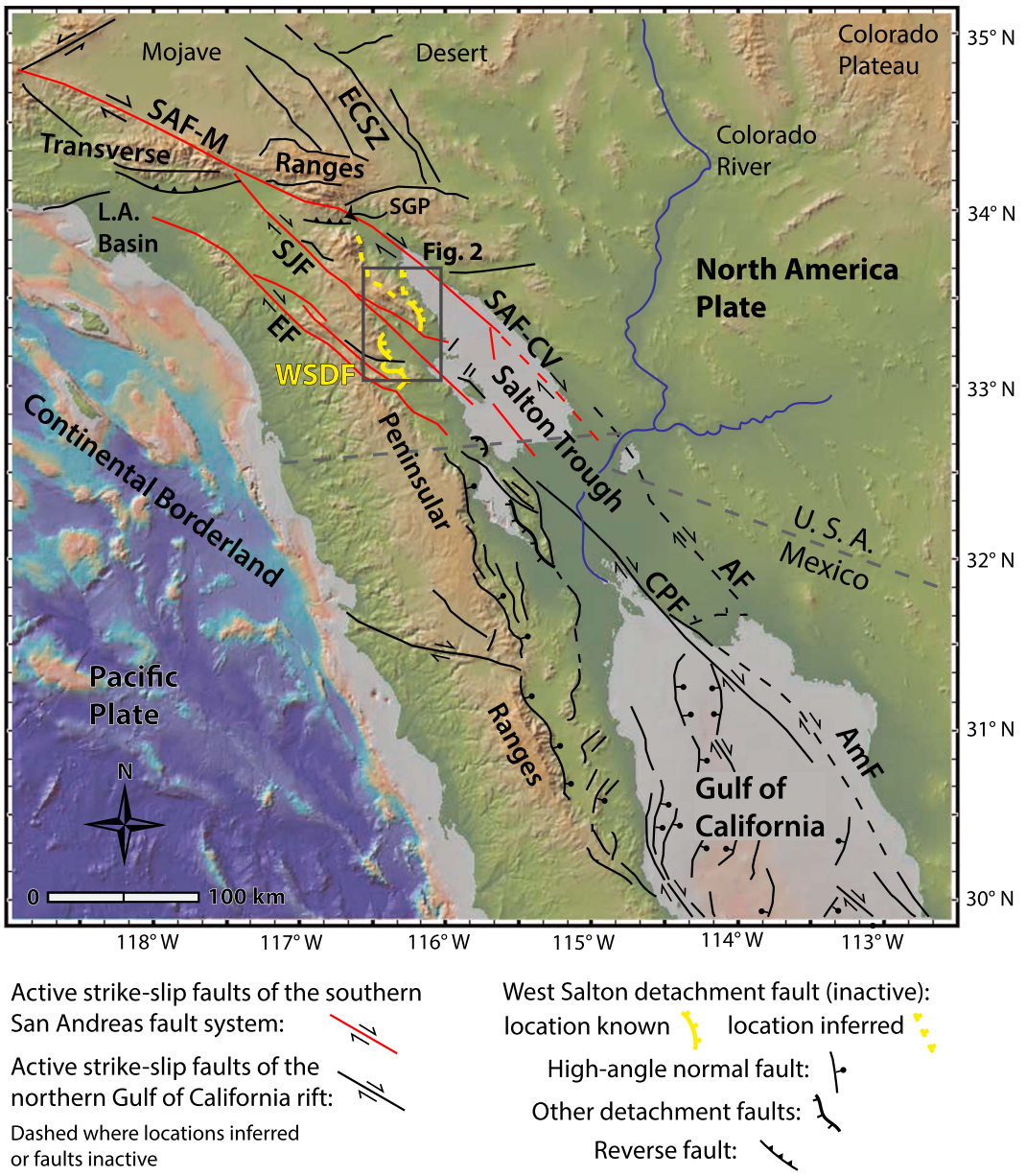

Figure 1. Shaded topographic relief and bathymetry of southern California and northwest Mexico (http://www.geomapapp.org) and simplified tectonic map showing southern San Andreas Fault zone and faults of northwest Mexico and the Gulf of California rift (Quaternary fault and fold database) (Dorsey & Lazear, 2013). Inset box outlines location of Figure 2. AF = Altar Fault, AmF = Amado Fault, CPF = Cerro Prieto Fault, EF = Elsinore Fault, L. A. = Los Angeles, SAF = San Andreas Fault, SGP = San Gorgonio Pass, SJF = San Jacinto Fault, WSDF = West Salton Detachment Fault.

plate boundary (Roeske et al., 2007). The northern Salton Trough in southern California (Figure 1) hosts the late Miocene southern San Andreas Fault (SAF) system, which includes the inactive West Salton Detachment Fault (WSDF) and the semiparallel active Coachella strand of the SAF. The WSDF and southern SAF in Coachella Valley were coeval structures (Axen & Fletcher, 1998; Dorsey et al., 2011); thus, the timing of extension initiation along the WSDF should inform us about the timing of plate boundary localization in the Salton Trough and the nature of the driving mechanisms.

The kinematics of plate boundary evolution within the Salton Trough (Figure 1)—the northern extent of the Gulf of California oblique rift—are debated, and several models have been proposed (summarized by Darin et al., 2016): (1) a model of strain partitioning between circa 12.5 and 6 Ma with orthogonal extension in the

region east of the future Baja California Peninsula and transform style deformation within the Continental Borderlands, followed by transform plate boundary localization in the Gulf of California rift post circa 6 Ma; (2) a distributed transtension model, where oblique rifting occurred between circa 12.5 and 6 Ma, followed by more focused dextral shear during plate boundary localization at circa 6 Ma; and (3) a model of progressive localization, with distributed dextral transtension between circa 12.5 and 8 Ma, followed by the progressive localization of dextral-strong oblique extensional and plate boundary strain into the Gulf of California shear zone circa 6–8 Ma (Bennet & Oskin, 2014; Bennett, Oskin, & Iriondo, 2013; Seiler et al., 2011; Stock & Hodges, 1989). Onset of major tectonic subsidence associated with plate boundary localization was synchronous along much of western Mexico between circa 6 and 8 Ma (Bennett et al., 2016; Dorsey et al., 2011; Pacheco et al., 2006; Seiler et al., 2013). The lack of well-documented timing for initiation of the WSDF—the major tectonic element of the western Salton Trough—precludes complete assessment of kinematic models for plate boundary localization and evolution in the Salton Trough.

Tectonic deformation in the Salton Trough has been interpreted in the context of plate boundary dynamics (e.g., Shirvell et al., 2009). Early back-arc extension in northwestern Mexico and southern California would have ended with the cessation of subduction along the plate boundary by circa 12.3–14 Ma (Atwater & Stock, 1998). Later, localization of dextral plate boundary deformation between the Salton Trough and northwestern Mexico is associated with a progressive clockwise rotation of relative Pacific-North America plate motions (Bennett et al., 2016). Marine incursion into the northern Gulf of California at circa 6.3 Ma implies linkage of previously separate oblique rift basins (Bennett et al., 2015, and references therein). Shirvell et al. (2009) suggested that extension and WSDF footwall exhumation started as early as circa 14–12 Ma, with rapid exhumation between circa 7 or 5 Ma and continuing through 2 Ma, nearly synchronous with onset of dextral strike-slip deformation along the southern SAF system (Matti & Morton, 1993). Dorsey et al. (2011) used paleomagnetism and stratigraphic evidence to show that syntectonic basin subsidence and related faulting initiated in the Salton Trough region at circa 8 Ma, thus questioning the previous interpretation for an earlier initiation age for the WSDF. These two studies call upon different tectonic models for the evolution of the southern SAF system, and thus, further improvement for the timing of WSDF initiation should help constrain this major tectonic event.

The kinematics of strain partitioning along the southern SAF in Coachella Valley (Figure 2) have influenced the late Cenozoic kinematics of the central Salton block (the area bound by the San Jacinto Fault Zone and the southern SAF in Coachella Valley; Figure 2) (Meade & Hager, 2005). Geological, geophysical, and geomorphological evidence reveal recent and active northeast tilt of the central Salton block, potentially driven by transpression and crustal loading along a northeast dipping SAF in Coachella Valley (Dorsey & Langenheim, 2015). Hypotheses regarding the late Cenozoic kinematic history of the central Salton block cannot be fully assessed, however, due to the lack of adequate strain markers in the WSDF footwall in the Santa Rosa Mountains (SRM). Documentation of the timing and rates of uplift and erosion of crustal-scale blocks elsewhere along the SAF system have proven to be informative regarding the nature of strain partitioning and evolving kinematic response to plate motion obliquity (e.g., Dorsey & Roering, 2006; Spotila et al., 2007; Spotila, Farley, & Sieh, 1998; Spotila & Sieh, 2000; Stockli, 2005).

In this study, we present new data from 29 samples of apatite U-Th/He thermochronometry (AHe), to elucidate early WSDF behavior and late Cenozoic kinematic history of the SRM and central Salton block. Our data support an interpretation for two phases of normal faulting in the SRM. First, we quantify the magnitude of vertical exhumation for the first phase of low-angle extension along the WSDF. Then, we demonstrate how the WSDF initiated coincident with the inception of the southern SAF transform system in the northern Salton Trough. Finally, we offer new constraints for the magnitude of late-stage high-angle extension along the Santa Rosa Fault and associated crustal-scale northeast tilting of the Santa Rosa Mountains during a regional tectonic reorganization of the southern SAF system.

2. Geologic Background

2.1. Regional Tectonic Setting

The southern SAF system (Figure 1) has a long history of kinematic complexity and regional fault system reorganization. Middle to late Miocene dextral plate boundary motion was focused west of Baja California along the continental borderlands and along proto-SAF strands northwest of Coachella Valley in the central and

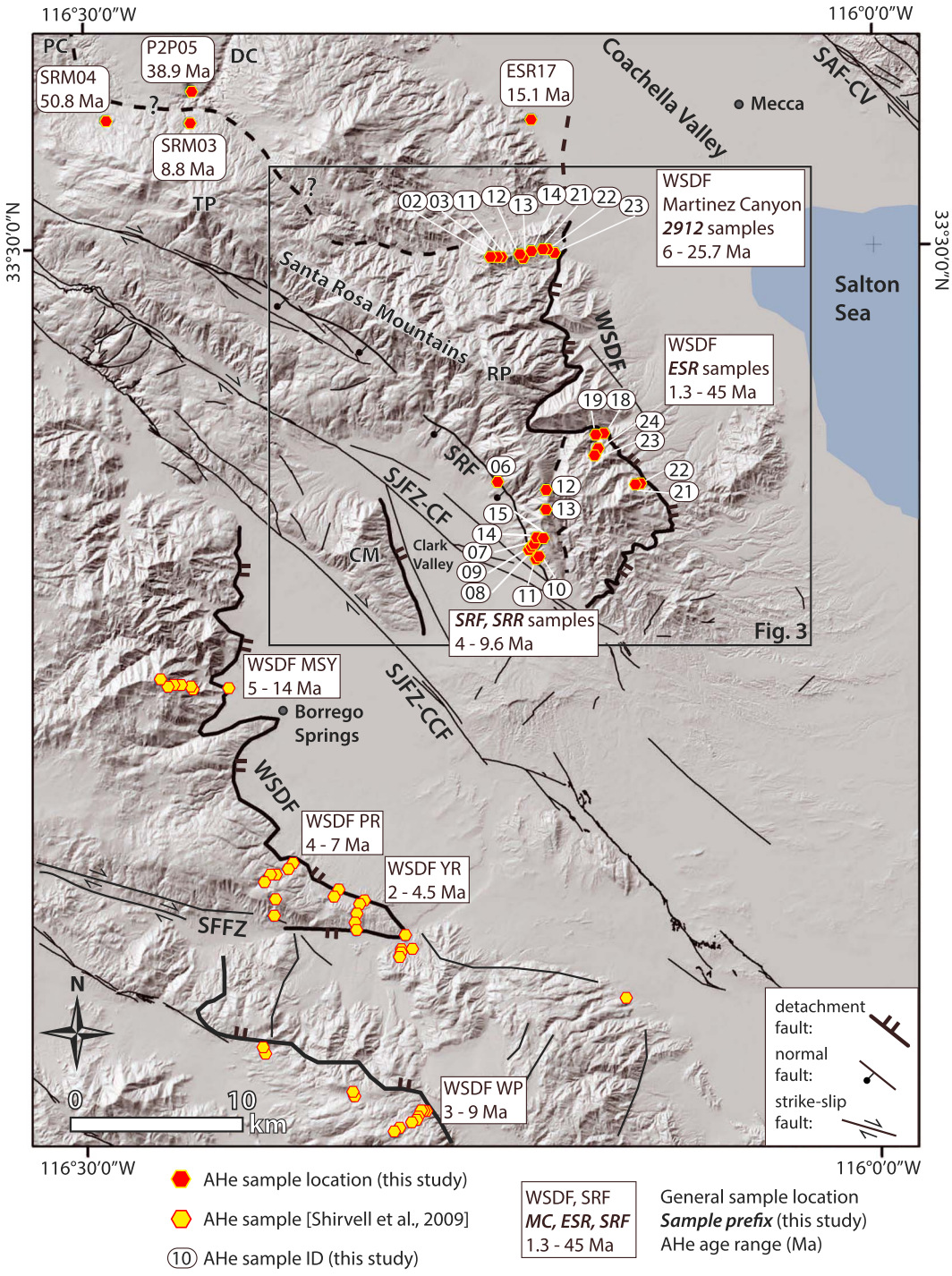

Figure 2. Shaded relief map and major faults of the Coachella Valley and western Salton Trough, California. Apatite U-Th/He (AHe) sample locations from Shirvell et al. (2009) in yellow and AHe sample locations from this study in red. Sample IDs in white boxes with round corners (see Table S1 in the supporting information for sample details). CCF = Coyote Creek Fault, ESR = eastern Santa Rosa, MC = Martinez Canyon, MSY = Mount San Ysidro, PR = Pinyon Ridge, RP = Rabbit Peak, SAF-CV = San Andreas Fault-Coachella Valley, SFF = San Felipe Fault, SJFZ-CF = Jacinto fault zone-Clark Fault, SRF = Santa Rosa Fault, SRR = Santa Rosa Ridge, TP = Toro Peak, WP = Whale Peak, WSDF = West Salton Detachment Fault, YR = Yaqui Ridge. Elevation data: U.S. Geological Survey National Map Viewer. Fault locations: Quaternary faults and folds database (Dorsey et al., 2011; Shirvell et al., 2009; Steely et al., 2009; U.S. Geological Survey (and California Geological Survey), 2006).

western Transverse Ranges (Bennet & Oskin, 2014; Buscher & Spotila, 2007; Matti & Morton, 1993; Powell, 1981; Spencer & Normark, 1979). By circa 6 Ma at least 90% of Pacific-North America dextral plate motion (Oskin & Stock, 2003) was concentrated in the Gulf of California shear zone, east of Baja California, and kinematically linked to the early southern SAF system (Figure 1) (Bennet & Oskin, 2014). The modern Gulf of California oblique spreading system transfers slip north to the southern SAF system through right-stepping faults in the southern Salton Trough (Figure 1). Within the Salton Trough, two major northwest striking fault zones carry the majority of dextral slip: the San Jacinto Fault Zone (SJFZ) and the Coachella strand of the southern SAF (Thatcher, Savage, & Simpson, 2016). The SJFZ is kinematically linked to the Mojave section of the SAF, whereas the Coachella segment of the SAF appears to transfer some of its slip to the eastern California shear zone (Thatcher et al., 2016). The SJFZ initiated at circa 1.2 Ma, as deduced from magnetostratigraphy and stratigraphic relationships along the northern SJFZ and to the southwest of our field area (Lutz et al., 2006; Morton & Matti, 1993).

The Salton Trough is a tectonically controlled depression and sedimentary basin defined by evolving structural elements of the southern SAF system. The northern terminus of the modern Salton Trough is San Gorgonio Pass (Figure 1), while the east and west are bound by the SAF and WSDF, respectively. San Gorgonio Pass represents a structural knot composed of the complex intersection of several fault systems (Langenheim et al., 2005). Initiation of the Elsinore and SJFZ may be a response to oblique convergence of the Baja California microplate in the region of the structural knot (Dorsey et al., 2012; Janecke et al., 2010; Kirby et al., 2007; Langenheim et al., 2005; Lutz et al., 2006; Steely et al., 2009). Collectively, the Elsinore and SJF zones reroute 25%–35% of plate boundary slip budget to the west around San Gorgonio Pass (Thatcher et al., 2016). The Coachella strand of the SAF accommodates between ~30 and 45% of total plate motion (Behr et al., 2010) and may transfer a significant portion of this plate motion (~12%–36%) east of San Gorgonio Pass to the eastern California shear zone and the Walker Lane (Thatcher et al., 2016, and references therein). Although the timing of SAF initiation in Coachella Valley is debated, strike-slip fault displacement in the Salton Trough was ongoing by circa 6–5 Ma (Crowell, 1981; Ehlig, 1981; Ingersoll & Rumelhart, 1999; Matti & Morton, 1993; Nicholson et al., 1994). Kinematic understanding of the initiation of early rifting and evolution of the modern SAF system in Coachella Valley is incomplete, however, and requires specific characterization of each stage and element of deformation.

2.2. West Salton Detachment Fault

The WSDF is the northernmost expression of a belt of north to northwest trending low- and high-angle extensional structures that occur over ~1000 km from southern Baja California to northern Coachella Valley (Axen, 1995). Low-angle normal faults in this system are interpreted to postdate Oligocene to middle Miocene low-angle structures of the Basin and Range (Axen & Fletcher, 1998). The WSDF has been mapped in at least two east dipping (~15°–20°) strands through the central and eastern SRM (Figure 2) (Axen & Fletcher, 1998; Matti et al., 2002).

Few studies have constrained the timing and kinematics of the WSDF (Axen & Fletcher, 1998; Dorsey et al., 2011; Shirvell et al., 2009). Axen and Fletcher (1998) favored a late Miocene initiation age that may have predated the active southern SAF in Coachella Valley, with slip ongoing through mid-Pleistocene time. Shirvell et al. (2009) used low-temperature thermochronometry (apatite and zircon He) on WSDF footwall and hanging wall rocks (~30 km southwest of the SRM) to assess the timing and magnitude of slip along the detachment system. A vertical transect (~1300 m) at Mount San Ysidro yielded AHe cooling ages that span circa 5–14 Ma (Figure 2) with no discernable evidence for a change in exhumation rate over that span of time. Farther south at Pinyon and Yaqui Ridge, fault-perpendicular traverses yield AHe ages that span circa 2–7 Ma, becoming younger in the hanging wall transport direction and indicating rapid late Miocene or Plio-Pleistocene cooling. The authors interpret (1) that the WSDF may have initiated as early as 14–12 Ma and (2) that rapid exhumation probably did not occur until circa 7 or 5 Ma and continued through circa 2 Ma. Paleomagnetism and stratigraphic analyses in the Fish Creek-Vallecito basin documented a minimum age for onset of strong extension and fault-bounded basins at 8.1 ± 0.4 Ma (Dorsey et al., 2011), potentially synchronous with the interpreted increase in WSDF slip rate at circa 7–5 Ma. The onset of earliest fault slip on the WSDF is still unclear from the available data, particularly in the northern Salton Trough where the SRM lack constraints, and exposed footwall rocks in the San Jacinto Mountains yield middle Miocene and older AHe cooling ages that predate WSDF-related extension (Wolf, Farley, & Silver, 1997). If the WSDF

initiated at circa12 Ma, the timing would fit with that of regional but distributed proto-Gulf extension, but an age of circa 8 Ma may indicate a very different plate tectonic driver for extension in the Salton Trough.

2.3. Central Salton Block and the Santa Rosa Mountains

The central Salton block contains abundant evidence of recent and active down-to-the-northeast tilting (Figure 3) (Dorsey & Langenheim, 2015). For instance, the southwest facing flank of the SRM in Clark Valley (Figure 3) has high-gradient slopes relative to the northeast SRM, exhibits faceted spurs on the SRF footwall, and has juvenile drainage systems with low alluvial fan-catchment area ratios, whereas the northeast flank of the SRM has a lower average hillslope gradient, no indication of active faulting on the WSDF, and contains relatively well-developed drainages with larger alluvial fan-catchment area ratios (Dorsey & Langenheim, 2015). The northeast SRM also display evidence for 1–1.5° of progressive tilting in late Quaternary fans relative to modern alluvial fans (Dorsey & Langenheim, 2015). The subsurface Coachella basin displays asymmetric deepening from southwest to northeast, with growth strata that dip up to ~8° east and terminate at the SAF (Fuis et al., 2012). These lines of evidence point to broad, down-to-the-northeast tilting of the central Salton block, potentially driven by transpressive loading on the steeply northeast dipping southern SAF (Dorsey & Langenheim, 2015). The kinematic implications of central Salton block tilting are uncertain because the local orientation of the SAF is not known. Some studies have implied or assumed a vertical southern SAF (Herbert & Cooke, 2012; Loveless & Meade, 2011; Luo & Liu, 2012; Meade & Hager, 2005; Nicholson et al., 2013; Smith-Konter & Sandwell, 2009), whereas other recent work suggests that the southern SAF may dip 60°–70° northeast (Fattaruso, Cooke, & Dorsey, 2014; Fuis et al., 2012; Lin, 2013; Lin, Shearer, & Hauksson, 2007; Lindsey & Fialko, 2013).

The SRM block is structurally bound on the southwest by the Santa Rosa Fault (SRF), a west dipping, high-angle (~67°) normal fault interpreted to merge at depth with the Clark strand of the SJFZ in a negative flower structure beneath Clark Valley (Dibblee, 1954; Dorsey & Langenheim, 2015; Dorsey & Roering, 2006; Janecke et al., 2010). Given the association between this high-angle normal fault and the negative flower structure, the age of the SRF is probably the same as that of the SJFZ or circa 1.2 Ma (Lutz et al., 2006, and references therein). Exhumation of the SRM is thought to be a product of two phases of extension: (1) late Miocene low-angle detachment on the WSDF along the northeast flank of the SRM and (2) Pleistocene high-angle normal faulting on the SRF along the southwest flank of the SRM related to a releasing geometry within the SJFZ (Dibblee, 1984; Dorsey & Langenheim, 2015; Matti et al., 2006).

The bedrock lithology of the SRM (Figure 3) is primarily Cretaceous crystalline plutonic, mylonite, and pre-Cretaceous metasedimentary rocks. Late Cretaceous top-to-the-east reverse slip produced the Eastern Peninsular Ranges mylonite zone, which strikes roughly parallel to the axis of the range and dips ~45°–65° northeast (Simpson, 1984). The eastern SRM preserve up to 1.4 km of uplifted nonmarine and marine, syntectonic and posttectonic late Neogene strata exposed in the hanging wall of the WSDF (Cox et al., 2002; King et al., 2002; Matti et al., 2002, 2006). Basal syntectonic stratigraphy on the northeast flank of the SRM may correlate to the Split Mountain Formation and thus may have been deposited before circa 6.3 Ma (Cox et al., 2002), but the base of this section remains undated in the SRM. The upper section correlates to the Canebreak Conglomerate, known locally as the Zosel sequence (Matti et al., 2002, 2006).

3. Methods

3.1. AHe Thermochronometry

Low-temperature thermochronometry can be used to constrain large-scale structural deformation and exhumation histories of tectonic blocks (Spotila, 2005; Spotila et al., 1998; Stockli, 2005; Wolf et al., 1997). Apatite U-Th/He thermochronometry (AHe) is based on radiogenic ^{4}He production during alpha decay of parent isotopes (^{238,235}U, ^{232}Th, and ^{147}Sm) in the apatite crystal lattice (Ehlers & Farley, 2003; Farley, 2000; Farley & Stockli, 2002). ^{4}He ingrowth and diffusion is temperature dependent, with total ^{4}He retention below ~40°C and total loss of ^{4}He retention above ~85°C (Wolf, Farley, & Kass, 1998). The range of temperatures where ^{4}He is only partially retained (~40–85°C) is referred to as the helium partial retention zone (HePRZ). Effective closure temperatures range from 65 to 70°C for standard Durango fluorapatite diffusion kinetics with a given cooling rate and grain size (Dodson, 1973; Ehlers & Farley, 2003; Farley, 2000). Alpha (α) ejection may decrease ^{4}He concentrations within $<$20 μm of grain boundaries and is thus corrected for (F_T correction)

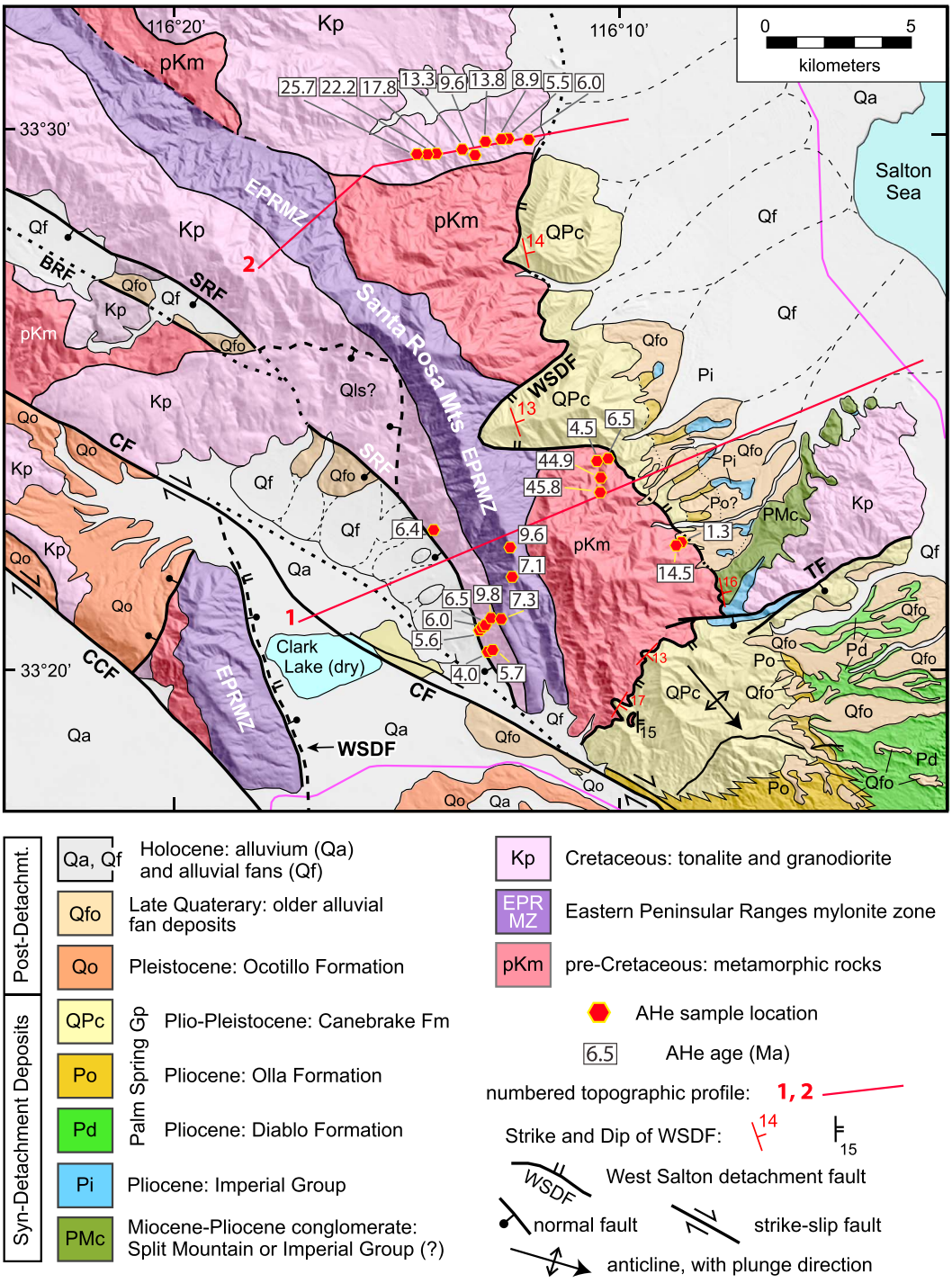

Figure 3. Detailed geologic map of the Santa Rosa Mountains with apatite U-Th/He (AHe) sample locations and ages and topographic profiles (modified from Dorsey & Langenheim, 2015). BRF = Buck Ridge Fault, CCF = Coyote Creek Fault, CF = Clark Fault, WSDF = West Salton Detachment Fault, TF = Travertine Fault. Geology compiled after Dibblee (1954), Sharp (1967), Todd, Erskine, and Morton (1988), Dorsey (2002), and Janecke et al. (2010).

using morphometric analysis and assuming homogeneous parent isotope distribution (Farley, 2000; Farley, Wolf, & Silver, 1996). In practice, closure temperatures of sample apatite depend on cooling rate, α-ejection, crystal size and morphology, and radiation damage (Brown et al., 2013; Dodson, 1973; Farley, 2000; Farley et al., 1996; Flowers et al., 2009; Shuster, Flowers, & Farley, 2006).

We collected 29 bedrock samples in vertical transects in the SRM, and we focus on three general locations along two range-bounding structures (Figure 2): (1) the SRF footwall in the southwest SRM ("SRF" and SRR samples), (2) the WSDF footwall in the southeast SRM ("ESR" samples), and (3) the WSDF footwall near Martinez Canyon in the central eastern SRM. We sampled structurally lowest locations along footwall localities at elevations between ~0 and 550 m above sea level (asl) and in vertical transects to elevations up to~1500 m asl. Sample lithologies included plutonic, Eastern Peninsular Range-type mylonites, and metasedimentary units (Figure 3). Generally, apatite yield and quality were high. We dated clear euhedral grains that were typically 65–100 μm in diameter.

Isotopic concentrations of apatites from our samples were primarily measured at Virginia Tech. However, Martinez Canyon ("2912") samples were processed and dated earlier at the University of Kansas. Single-grain and multigrain aliquots of apatite (typically three to six aliquots per sample, with one to four grains per aliquot) were hand-picked under cross-polar magnification to avoid defects in morphology or inclusions. When possible, aliquots consisted of apatite grains >70 μm in diameter; however, scarce or small apatite in only a few samples required measurement of aliquots with diameters <60 μm. Aliquots were loaded into Pt envelopes and degassed twice in a resistance furnace to 940°C for 20 min. ^{4}He was measured by quadrupole mass spectrometry and ^{3}He spike method. Blank levels for ^{4}He detection were ~0.2 fmol. Radiogenic parent isotopes (^{238}U, ^{235}U, ^{232}Th, and ^{147}Sm) were measured at the University of Arizona by isotope dilution and inductively coupled plasma mass spectrometry (Spotila & Berger, 2010). Effective Uranium (eU) content of aliquots ranged from ~10 to 200 ppm. We note only several instances where positive or negative age-eU correlation occurred; however, reproducibility in those samples typically was not affected.

Predicted age uncertainty is ~5% (1σ) based on instrument precision, F_T calculations, and error in alpha-ejection correction factors (Farley, 2000). Accuracy was checked against standards including Durango fluorapatite. Reported AHe age uncertainties are the standard deviation (1σ) of the replicate analyses (Table S1 in the supporting information); however, if standard deviation was <5%, an error of 5% was assigned. Age results were assigned as outliers if a calculated AHe age was >50% higher than other aliquots from the same sample. A total of 12 of 80 aliquots were assigned as outliers (see red italicized text in Table S1). The average standard deviation for all sample aliquots is 14.5% (after discarding outlier aliquots and assigning 5% uncertainty to samples with <5% standard deviation). Samples processed at the University of Kansas were measured and ages calculated using the same basic methods as above, and as explained in Shirvell et al. (2009). Analytical uncertainty was 3% (1σ) for these samples; however, none had standard deviations<3%, and thus, reported uncertainties are based on the variance of sample aliquot ages.

3.2. Thermal History Modeling

We used the software QTQt (Gallagher, 2012) to perform inverse thermal history modeling of vertical transects from the WSDF footwall in Martinez Canyon and the SRF footwall. Samples from the southeast SRM (ESR samples) were not modeled. QTQt uses Bayesian transdimensional Markov Chain Monte Carlo simulations that incorporate prior thermal and geological constraints. Early thermal history constraints for the Peninsular Range batholith are derived from U-Pb dating of zircons and ^{40}Ar/^{39}Ar dating of biotite, muscovite, and K-feldspar (Axen et al., 2000; Grove, Lovera, & Harrison, 2003). We modeled monotonic cooling of two vertical transects using a Monte Carlo simulation with 100,000 burn-in and 100,00 post-burn-in acceptable temperature-time paths. We allowed a range in geothermal gradient of 20–30°C/km and a surface temperature of 10 ± 10°C. Previous studies assign regional modern and paleogeothermal gradients that fall within the range we use to model thermal histories (Dumitru, 1990; Grove et al., 2003; Seiler et al., 2011; Shirvell et al., 2009; Spotila et al., 1998). Seiler et al. (2011) determined an Eocene geothermal gradient of 20–25°C/km in northern Baja California and argued that transient slab window heating should not have affected initial conditions of rifting in the northern Gulf Extensional Province. We modeled exhumation histories for both transects over a duration of 50 Myr.

4. Results

4.1. Apatite U-Th/He Thermocronometry

All sample locations, isotopic data, and resulting ages are available as supporting information in Table S1 and are discussed further in the following sections. AHe samples from the SRM generally display a strong positive

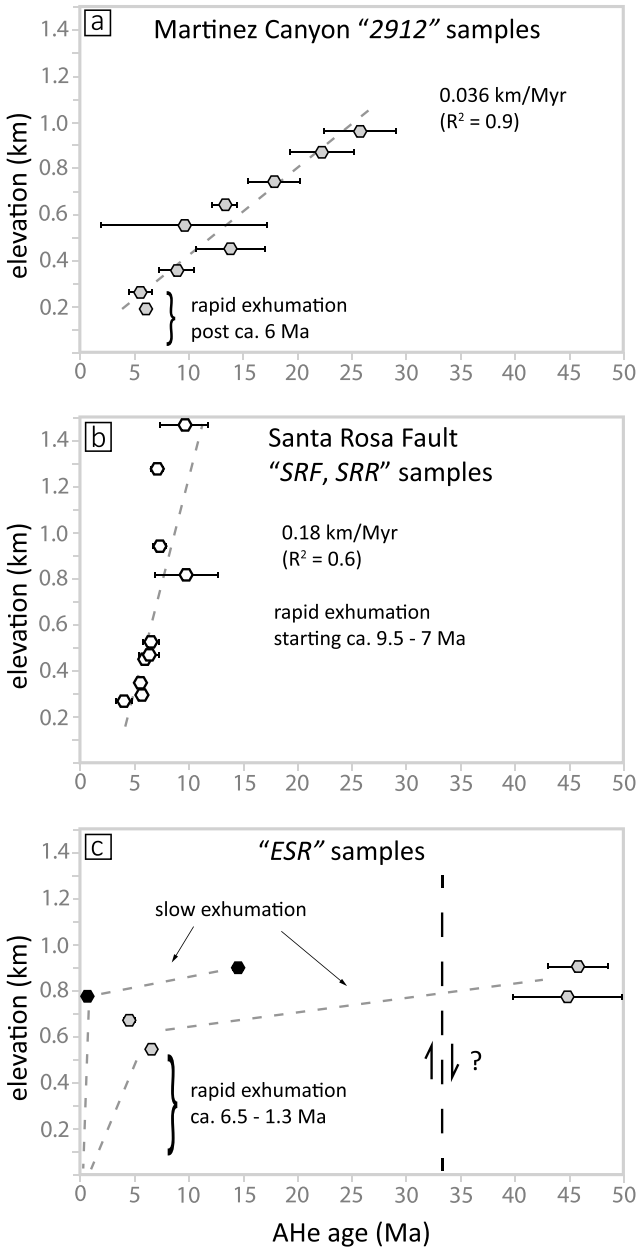

Figure 4. Elevation-age plots for samples of apatite U-Th/He (AHe) from the Santa Rosa Mountains (SRM). (a) Elevation-age relationship for samples from Martinez Canyon (MC; "2912" samples) along the West Salton Detachment Fault (WSDF) footwall, central eastern SRM. (b) Samples from the Santa Rosa Fault (SRF and SRR samples) footwall in the southwest SRM. (c) Samples from the southeastern Santa Rosa Mountains along the WSDF footwall (ESR samples). Note that ESR samples are divided into two short vertical transects; the north transect is represented by gray shaded hexagons, while the south transect is represented by black hexagons. See text for discussion of elevation-age relationship and possible structural complexity at this location. All error bars are standard deviations (1σ) of sample replicates.

correlation between elevation and age (Figures 3 and 4). Older AHe cooling ages at high elevations and high structural positions are consistent with regional cooling histories of Peninsular Range footwall blocks (Figure 4) (Grove et al., 2003; Shirvell et al., 2009; Wolf et al., 1997). In general, our ages become younger as elevation decreases, and the youngest AHe cooling ages (4.0–1.3 Ma) occur at low elevations and low structural positions in the SRM.

In the northern SRM, ~25 km northwest of Martinez Canyon, three samples across a possible ~east-west oriented strand or continuation of the WSDF yield footwall ages of 50.8 ± 5.4 Ma and 8.8 ± 0.7 Ma, while the lone hanging wall(?) sample yields an age of 38.9 ± 3.5 Ma (Figure 2). The extreme age variability of adjacent samples (8.8 to 50.8 Ma) along the potential footwall of this fault is difficult to explain (Figure 2). The interior of the northern SRM contains steep topography with faceted spur-like morphology suggesting the presence of a northeast dipping fault within the footwall of the WSDF. In light of this unresolved structural problem, we focus on the AHe sample ages from the central and southern SRM to elucidate the exhumation history of the range.

In the central eastern SRM, a vertical transect up the WSDF footwall in Martinez Canyon yields AHe sample ages of circa 5.5 ± 1.1 Ma and 6.0 ± 0.3 Ma at low elevations (190–260 m asl), while sample ages generally increase with elevation to 25.7 ± 3.3 Ma at the highest structural position (960 m asl; Figures 3 and 4a). The elevation-age relationship for samples from Martinez Canyon gives a gradient of ~0.036 km/Myr (R^2 = 0.9), with samples younging in the direction of footwall transport. Two samples from the lowest elevations and structural level suggest a steeper elevation-age gradient (Figure 4a).

Samples from the southwest SRM along the SRF footwall define a strong elevation-age relationship (Figure 4b). Sample ages increase from 4.0 ± 0.7 Ma at low elevation (270 m asl) and low structurally position up to 9.6 ± 2.15 Ma at high elevation (1473 m asl) and high structural position along the ridge line. Together, the SRF samples define an elevation-age gradient of 0.18 km/Myr (R^2 = 0.59; Figure 4b).

Samples from the southeast SRM (ESR samples) represent two short vertical transects (Figure 4c). While some deviation from elevation-age relationship may be expected with multikilometer-scale lateral offset along a fault footwall, we note a significant deviation from expected elevation-age relationships for these samples. Here sample ages range from 1.3 ± 0.1 Ma to 44.9 ± 10.1 Ma. As a result of inconsistent elevation-age relationships, or possible unnoted structural complexity, the elevation-age gradient for ESR samples is difficult to assess; our interpretation of these ages is a steep gradient between ca. 1.3–6.5 Ma, with a much lower gradient between >6.5 and 14 Ma and older. This interpreted pattern for ESR samples is consistent with observations from the elevation-age gradient from Martinez Canyon where samples display low gradients from circa 25 Ma to circa 6 Ma and a very steep gradient after circa 6 Ma.

SRF footwall samples do not appear to display the break in slope indicative of the initiation of faulting (Figure 4b). Thus, either the material that preserved an inflection was eroded from above the transect or possibly the break in slope is represented between samples with ages of circa 7–10 Ma (Figure 4b). The

range of initiation timing suggested by the results of our AHe ages may be narrowed by employing quantitative thermal modeling (Gallagher, 2012; Ketcham, 2005).

5. Discussion

Analyses of the 3-D spatial patterns of AHe age results from the SRM indicate an abrupt increase in cooling rates beginning between circa 6 and 9.5 Ma, in the late Miocene (Figure 4). Available structural data indicate that late Miocene cooling was caused by tectonic exhumation along the low-angle WSDF in the eastern SRM. A second phase of tectonism along the southwest flank of the SRM during the early Pleistocene (circa 1.2 Ma) (Janecke et al., 2010; Lutz et al., 2006) exhumed a structurally lower section of WSDF footwall via slip on the high-angle SRF. The geomorphology of the SRM, including catchment and fan areas, relative steepness and relief, gravity data and subsurface geometries of strata in Coachella Valley (Dorsey & Langenheim, 2015; Fuis et al., 2012), along with the timing of SJFZ initiation (Janecke et al., 2010; Lutz et al., 2006), provide constraints on the direction and magnitude of late-phase tectonic exhumation, extension, and down-to-the northeast crustal tilting of the SRM.

In the following sections, we present interpretations of thermochronologic data from across the SRM block. Tilt corrections to AHe data allow thermal history analyses that improve the constraints for timing of initial WSDF slip. We then discuss constraints for the magnitudes and rates of extension and vertical exhumation in the SRM within a regional tectonic context. Finally, we discuss the implications of different geologic rates related to each phase of normal faulting in the context of plate tectonics and local fault geometry associated with the evolution of the southern SAF system.

5.1. Post-WSDF Tilt Corrections

5.1.1. Constraining Down-to-the-Northeast Tilt of the Santa Rosa Mountains Using AHe Isochrons

Pleistocene high-angle normal faulting along the SRF was not sufficient to exhume reset AHe ages to surface elevations (SRF and SRR samples; Figure 3). Still, asymmetric Pleistocene-to-recent deformation of the central Salton block effectively enhanced the vertical exhumation of the southwest SRM and resulted in tilted Miocene isochrons (Figure 5). The approximate elevations of late Miocene isochrons in three locations across the SRM may be used to quantify the degree of post-Miocene tilting using a three-point approach. Results of this exercise in the SRM using AHe isochrons can then be compared to numerous independent estimates for northeast tilting of the central Salton block (e.g., Dorsey & Langenheim, 2015).

To define the attitude of post WSDF tilting of the SRM, we projected the 9 Ma isochron just above the circa 8.9 Ma AHe sample age that occurs in Martinez Canyon at ~360–555 m asl, to the south below the circa 9.6 Ma AHe sample age in the SRF footwall between ~1280 and 1470 m asl. Then we projected the 9 Ma isochron from the SRF footwall toward the northeast to between the circa 6.5 Ma and circa 14 Ma AHE sample ages, at elevations of ~600–850 m asl (ESR samples). We find that the 9 Ma isochron has a strike of ~295–320° and a dip of ~6–12° northeast. We note that it is impossible to recognize or rule out crustal-block scale warped or convex-up isochrons with the resolution of our thermochronologic data.

Tilting of the central Salton block by at least 5° northeast is consistent with results from several other workers (Dorsey & Langenheim, 2015). An identical geometry of tilting for the central Salton block is indicated by catchment-and fan-area relationships for the southwest and northeast SRM and by gravity data showing progressive northeast deepening of sedimentary fill toward the SAF in Coachella Valley (Langenheim et al., 2005). Subsurface stratigraphic patterns below the Salton Sea in Coachella Valley indicate that Quaternary growth strata dip ~5–8° northeast and thicken toward the SAF (Fuis et al., 2012). And late Neogene sedimentary units in the eastern SRM have been uplifted and tilted northeast (Cox et al., 2002; Matti et al., 2002, 2006).

5.1.2. Applying Tilt Corrections to AHe Sample Elevations

Correcting for post-1.2 Ma tilt allows us to (1) improve thermal history modeling of late Miocene exhumation and (2) constrain SRF-related exhumation magnitude and rate using the geometric consequences of tilt correction. We chose to correct for a value of 8° of post early Pleistocene northeast tilt of the SRM block. We projected samples from the SRF and Martinez Canyon onto a single topographic profile orthogonal to the central SRM (i.e., Profile 1 in Figure 3) and then applied a simple rotation matrix to calculate changes in sample elevations along the profile. We chose a fulcrum of tilt (the origin in our rotation correction) within the modern alluvial fans on the eastern bajada of the SRM (after Dorsey & Langenheim, 2015).

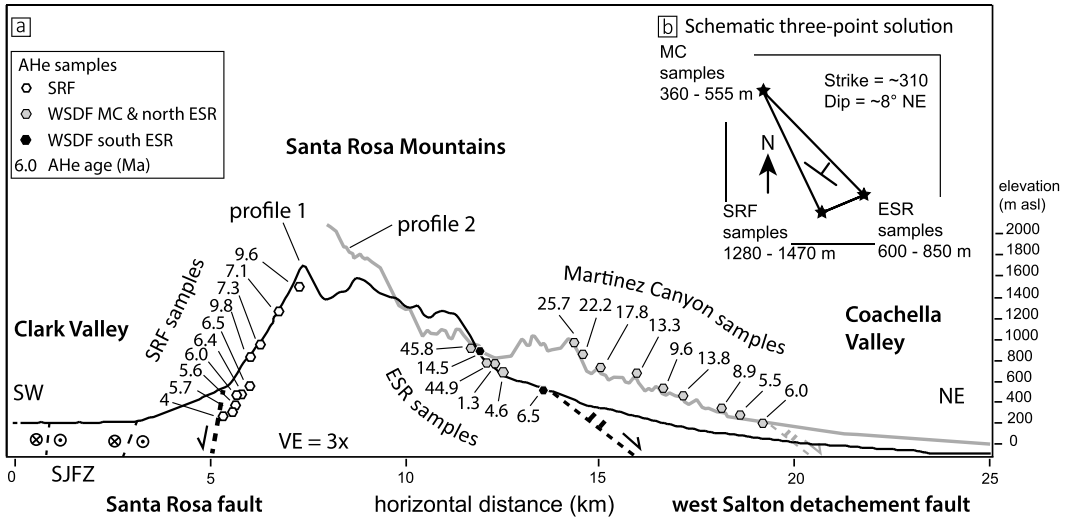

Figure 5. (a) Topographic profiles across the southern and central Santa Rosa Mountains (SRM) with projected sample locations and apatite U-Th/He (AHe) cooling ages in millions of years ago. Locations for profiles are found in Figure 3. Note that samples from the southeastern SRM are divided into two short vertical transects (see Figures 3 and 4c). (b) Inset schematic three-point solution for the circa 9 Ma AHe isochron using sample elevations and locations in this study. See text for details of three-point construction. SJFZ = San Jacinto Fault Zone, SRF = Santa Rosa Fault, VE = vertical exaggeration.

To correct sample elevation spacing for thermal modeling, we pinned the base of each tilt-corrected transect to the modern elevations of each lowest sample in a transect. We then calculated the new vertical offset between each overlying sample using the tilt-corrected elevation offsets. Only the vertical positions of samples overlying the lowest samples were adjusted.

For the second application of the tilt correction, we utilized the estimates of *total* vertical offset of all samples —a geometric consequence of the rotation correction—to constrain the circa 1.2 Ma paleodepths of each transect (SRF, Martinez Canyon) and thus estimate SRF-related vertical exhumation. An important result of this correction is that samples farther from the fulcrum, e.g., SRF samples, experienced a greater vertical shift than those close to the fulcrum.

Tilt corrections result in lower elevation-age gradients for both Martinez Canyon and SRF transects and improve the internal consistency of paleoelevation-age relationships across the SRM block. A tilt-corrected Martinez Canyon transect has a corrected gradient of 0.012 km/Myr (R^2 = 0.88), and a corrected SRF transect has a new gradient of 0.15 km/Myr (R^2 = 0.54). The tilt-corrected zero-age depth (see Spotila, 2005) for the SRF transect is~2.1 km depth, compared to only 0.55 km depth in the uncorrected transect. Tilt-corrected sample paleodepths place the highest SRF samples at similar paleodepth positions to those of the lowest Martinez Canyon samples.

5.2. Thermal History Modeling

Quantitative thermal modeling is commonly used to complement and assist with the interpretation of results of AHe elevation-age data (Gallagher, 2012; Ketcham, 2005). We construct temperature-time (T-t) paths for inverse thermal history models of multisample vertical transects from the WSDF and SRF footwalls (Figure 6). ESR samples were not used in quantitative thermal history modeling due to their relatively poor elevation-age relationships. This configuration of samples from low- and high-angle normal fault footwalls affords a thermal perspective for the WSDF footwall and insight into the thermal history of the SRM block.

Inverse model results from transects in Martinez Canyon (WSDF footwall), and the SRF footwall indicates synchronous and rapid late Miocene cooling beginning at circa 8 Ma at a rate of 5–6°C/Myr (Figure 6). Samples from Martinez Canyon (n = 9 samples) may have resided within the HePRZ during early Miocene time (Figure 6a), while the modeled T-t path also indicates a thermal history involving more rapid cooling from

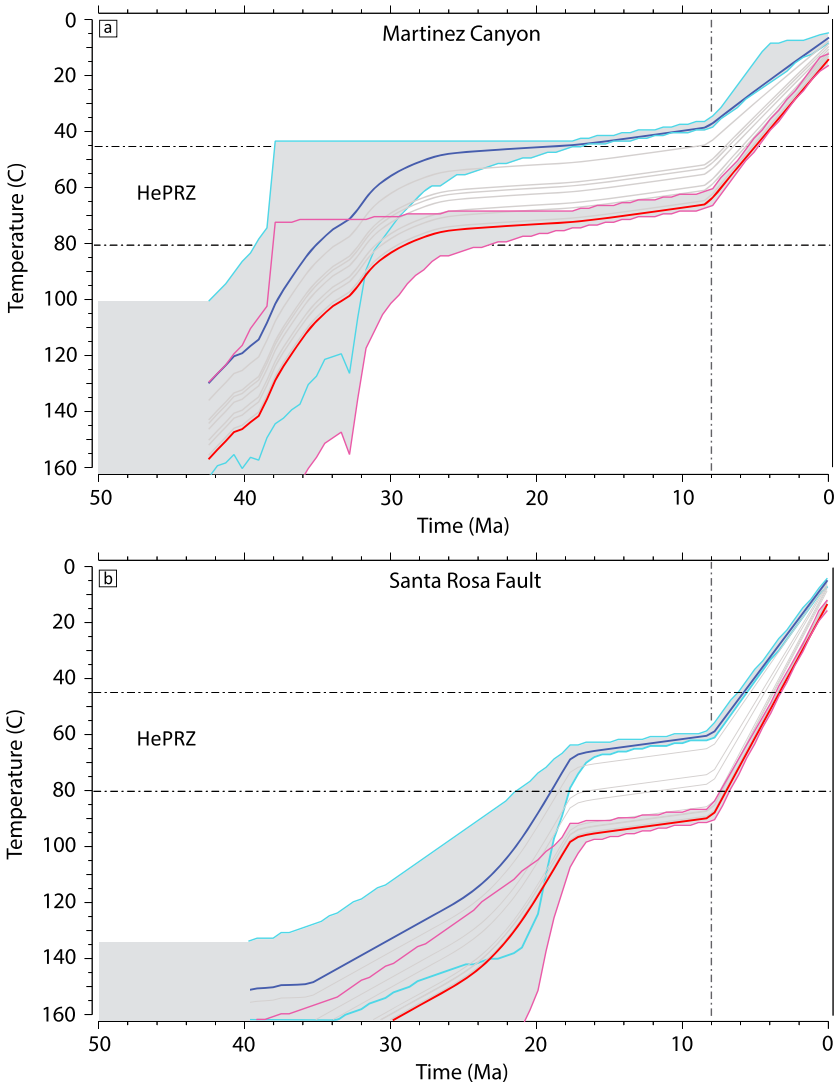

Figure 6. QTQt thermal history model results for apatite U-Th/He (AHe) samples from the Santa Rosa Mountains (SRM). Red and blue colored lines represent model space constrained by our AHe data. (a) Inverse model results showing best fit temperature-time (*T-t*) histories for samples from Martinez Canyon ("2912" samples). (b) Inverse model results showing best fit *T-t* histories for samples from the Santa Rosa fault footwall (SRF and SRR samples) in the southwest SRM. Red and blue lines represent structurally lowest and highest samples, respectively. Gray shaded areas with magenta and teal bounds are 95% confidence envelopes, for structurally lowest and highest samples, respectively. Intermediate gray lines represent other sample paleodepths/temperatures (no 95% confidence envelopes are shown for these). Pre-Miocene thermal constraints in model from Grove et al. (2003). HePRZ = He partial retention zone. Vertical dashed lines delineate onset of late Miocene cooling starting at 8 Ma.

early Eocene through mid-Oligocene time (circa 42–28 Ma), a thermal event that has been documented throughout the Eastern Peninsular Ranges (Axen et al., 2000, and references therein). However, the oldest aliquot age for the Martinez Canyon transect is circa 28 Ma, and the confidence envelopes are consistent with slow or rapid pre-Miocene cooling. Samples remained isothermal after circa 27 Ma.

Inverse model results from the SRF footwall in the southwest SRM (n = 10 samples) display a T-t path indicating moderate or slow cooling between circa 40 Ma and 18 Ma (Figure 6b), through the early and middle Miocene, followed by ~10 Myr of isothermal or very slow cooling (<1°C/Myr). Starting at 8 Ma, the cooling rate increased to 8–9°C/Myr and continued through the Pleistocene (Figure 6b, SRF and SRR samples). The structurally lowest four to six samples likely resided below the HePRZ during early Miocene to earliest late Miocene time, and thus, their cooling ages reflect rapid vertical advection through the HePRZ.

While the independent T-t paths agree on synchronous onset of late Miocene cooling, there is a slight discrepancy in cooling rates. Inverse model results from Martinez Canyon show a T-t path that indicates slower cooling (~5–6°C/Myr) than the cooling rate derived from the T-t path for the SRF samples (~8–9°C/Myr). Potential causes for discrepancies in the inverse models include possible local variability in geothermal gradient, variation in elevation, nonuniform tilt of the SRM, and possible local structural complexities. Another potential influence on the T-t paths could be the interpreted long duration of residence in the HePRZ for Martinez Canyon samples (Figure 6a). Nevertheless, the model results taken together indicate a broadly self-consistent thermal history for the SRM block.

5.3. Late Miocene (Circa 8 Ma) Onset of WSDF Footwall Exhumation

Elevation-age relationships (Figures 4 and 5) and thermal history modeling (Figure 6) demonstrate tectonic exhumation of the SRM along the WSDF most likely commenced at circa 8 Ma. We illustrate the evolution of the SRM beginning in the late Miocene through recent times using conceptual tectonic block diagrams and thermochronometric data from our study (Figure 7). Our preferred age of circa 8 Ma for initiation of the WSDF is consistent with onset of extension and WSDF-controlled basin formation deduced from stratigraphic records on the northeast flank of the SRM (Cox et al., 2002) and paleomagnetism of basal stratigraphic units in the Fish Creek-Vallecito basin; (Dorsey et al., 2011). Our result is also consistent with studies in the northern Gulf of California that date onset of extension (as well as clockwise block rotations and development of strike-slip faults) related to strong regional transtension at circa 7–9 Ma (e.g., Bennett et al., 2013, 2016; Seiler et al., 2013).

The relatively deeper paleodepth of the SRF transect compared to the Martinez Canyon transect, as inferred from tilt-corrected elevation-age data, is supported by thermal modeling results (Figure 6). These thermal history model results also provide estimates for pre-late Miocene paleodepths of sample transects (Figure 6). SRF samples cooled from temperatures as high as 90–100°C since the late Miocene, while samples from the eastern SRM, collected near the low-angle WSDF plane surface, were likely within the HePRZ or near the base of the HePRZ (~80–65°C) before late Miocene fault initiation (Figure 7g). This configuration is consistent with the relatively lower topographic relief along the Martinez Canyon transect (Figure 5), the relatively lower elevation-age gradient of the Martinez Canyon transect (Figure 4b), and the relatively lower tilt-corrected elevation-age gradient from Martinez Canyon (Figure 7b). Another result of this configuration is an apparent increase in spacing between the isochrons from the SRF transect compared to those from Martinez Canyon, which have a smaller spacing, probably due to prolonged residence in the HePRZ (e.g., Stockli, 2005).

Young AHe ages from the southeast SRM (ESR samples) also record extension-related cooling during the late Miocene and continuing through the Pleistocene (i.e., 6.5, 4.0, and 1.3 Ma). However, a lack of monotonic elevation-age relationships precludes a robust slip history analysis or thermal modeling of AHe sample ages from the southeast SRM. Late Miocene through Pleistocene AHe ages do support a model of WSDF-related tectonic denudation of the southeastern SRM from depths of at least ~2.2 km since 6.5–1.3 Ma (Figure 4c).

5.4. Rates and Magnitudes of Exhumation

Rates of vertical exhumation along the low-angle WSDF aid reconstructions of the insipient plate boundary in Coachella Valley, but assigning rates and magnitudes of slip to the WSDF depends upon the measure of cooling, and there are several possible scenarios that should be examined. Elevation-age gradients yield a measure of long-term vertical exhumation associated with the WSDF. For the SRF transect, this rate is ~0.15 km/Myr (tilt corrected) since WSDF initiation. The elevation-age gradient for Martinez Canyon is low due to residence in the HePRZ and tells us little about exhumation rate. However, a second measure of vertical exhumation uses the results of our thermal history models, which show cooling rates of ~5–9°C/Myr (Martinez Canyon and SRF footwall, respectively), translating to vertical exhumation rates of 0.20–0.36 km/Myr, from depths of up to 3.2 km (paleotemperature of ~90°C; Figure 6b). Yet a third approach uses apatite closure temperature estimates to constrain rates of vertical exhumation. For all SRF and ESR samples, we calculated a mean closure temperature of 65°C ± 4°C (1σ standard deviation of the variance) (after Ehlers & Farley, 2003; Farley & Stockli, 2002; Wolf, Farley, & Silver, 1996; Wolf et al., 1998). We then used a geothermal gradient of 25°C/km, a closure temperature depth of 2.2 ± 0.2 km, and estimates of post-WSDF sample paleodepth (tilt-corrected) and AHe cooling ages to calculate rates of time-averaged vertical uplift

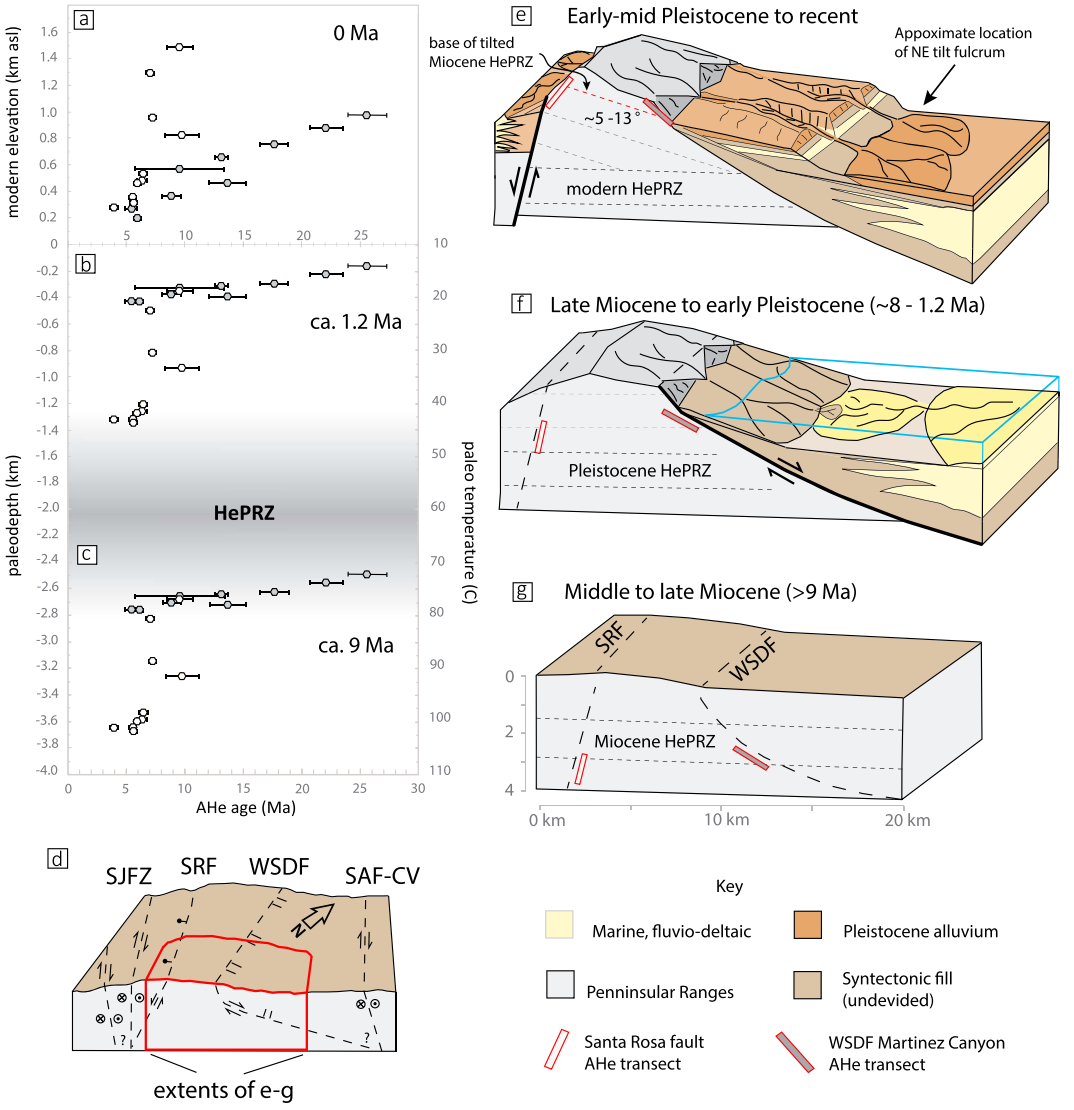

Figure 7. Evolution of Miocene to present elevation-age relationships for samples from the Santa Rosa Mountains (SRM) with structural block diagrams for each relevant time step. (a) Modern sample age-elevation relationships for samples form the SRM. White hexagons are samples from the Santa Rosa fault (SRF). Gray filled hexagons are from the West Salton Detachment Fault (WSDF) footwall in Martinez Canyon. (b) Pre-WSDF tilt-corrected elevation-age relationships (see text for details). (c) Predetachment paleodepth and paleotemperature reconstruction for WSDF footwall rocks. (d) Block diagram showing schematic tectonic configuration between the San Jacinto (SJFZ) and the Coachella segment of the San Andreas Fault (SAF-CV). (e and f) Evolution of the WSDF-SRF system interpreted from our thermochronologic results. Sample transect locations denoted by red outlined rectangles along west and east flanks of SRM. Active faulting during any time step is indicated with a bold black line and relative motion arrows. Incipient faults are thin, dashed black lines. Previously active(inactive) faults in any timeframe are thin black lines (e.g., WSDF in Figure 7e). Figure 7e shows the modern configuration of the SRM block, including active SFR and inactive WSDF. Location of NE tilt fulcrum from Dorsey and Langenheim (2015) and discussed in section 5.1.1. Figure 7f shows active to postdetachment phase of the SRM, showing deposition of coarse-grained alluvial fans and marine to fluvio-deltaic deposits derived from the uplifted footwall, Gulf of California seaway, and the Miocene-Pliocene Colorado River system. Figure 7f shows detailed schematic predetachment configuration. Location of block diagrams within SRM is similar to topographic profile 1 in Figure 3.

(after Stockli, 2005; Spotila, 2005). The results are minimum vertical exhumation rates between ~0.15 and 0.22 km/Myr for structurally low samples from the SRF footwall. The use of non tilt-corrected, modern sample elevations yield rates between 0.4 and 0.6 km/Myr, somewhat higher than those derived from elevation-age gradients, *T-t* paths, and closure technique using post-WSDF tilt-corrected sample

paleodepths. The remarkable similarity between rates using the first three techniques may indicate that time-averaged vertical exhumation along the WSDF was between 0.15 and 0.36 km/Myr, from circa 8 Ma through the inception of the SJFZ at circa 1.2 Ma.

Low to moderate rates of vertical exhumation since circa 8 Ma may not necessarily reflect slow fault slip rates. We used geometric relationships between vertical exhumation rate and assumed fault dip to calculate coarse slip rate estimates for the WSDF. The distribution of WSDF dips measurements along the eastern SRM cluster near 15° to the northeast (Figure 3), and restoration of Pleistocene tilting results in a shallower dip of ~7°. Using this configuration, fault slip rates were likely ~1.2–3.0 km/Myr in a direction orthogonal to the SRM block (azimuth of ~060°–080° northeast).

Rocks from the southwestern SRM (SRF transect) cooled through the HePRZ starting in the late Miocene through Pleistocene during footwall uplift related to slip on the WSDF from depths >3 km (Figures 7g and 7f), but probably resided within the upper 1.5 km of Earth's crust until they were further exhumed by slip on the high-angle SRF beginning at circa1.2 Ma (Figures 7f and 7e) (Dorsey et al., 2012; Janecke et al., 2010; Kirby et al., 2007; Lutz et al., 2006; Steely et al., 2009). AHe ages exposed at the surface were not reset by exhumation on the SRF and therefore do not reflect the youngest phase of tectonism. However, using the same estimates for tilt-corrected post-WSDF paleodepth, we may constrain the early Pleistocene to present rate of exhumation on the SRF (Figure 7). The lack of Pleistocene AHe exhumation ages suggests that we may rule out exhumation from depths below the closure temperature of apatite (>2.2 km), which agrees with our maximum tilt-corrected sample paleodepths of ~1.4 km for samples from the SRF. Our estimate for ~1.4 km of Pleistocene slip on the SRF also agrees with interpretations from a gravity profile across Clark Valley showing only ~1 km of sediment in the SRF hanging wall (Dorsey & Langenheim, 2015). If the lowest samples along the SRF were exhumed to their modern elevations from a tilt-corrected paleodepth starting at 1.2 Ma, the range of vertical exhumation rates is then ~1.3–1.4 km/Myr. An independent slip rate estimate based on faceted-spur morphology of the SRF footwall brackets our estimate at 0.5–2.0 km/Myr (Dorsey & Langenheim, 2015; after dePolo & Anderson, 2000).

Rates of vertical exhumation in the SRM yield new insights into the kinematics of two extensional fault systems operating over two timescales: (1) initiation of WSDF resulted in relatively slow to intermediate vertical exhumation rates of ~0.15–0.36 km/Myr in the SRM (footwall of the WSDF), between circa 8 and 1.2 Ma, and (2) vertical exhumation rates along the southwestern flank of the SRM increased at least threefold to ~1.3 km/Myr during initiation of the SJFZ and SRF. The total vertical exhumation attributable to slip on the WSDF, as constrained by interpretations of the Miocene HePRZ and thermal modeling, was ~3.2 km for the crustal section sampled in the southwest SRM and closer to 2.2 km for samples from Martinez Canyon. Relatively higher vertical exhumation in the southwest SRM is due to post-WSDF slip on the SRF and to the greater distance from the fulcrum of northeast tilt located in western Coachella Valley.

5.5. Implications

Correction of recent down-to-the-northeast tilting and thermal history modeling of sample transects on the east and southwest flanks of the SRM (Martinez Canyon and the SRF, respectively) reveal an internally consistent exhumation history for the SRM beginning at circa 8 Ma through present. Initiation of the WSDF and southern SAF system at circa 8 Ma occurred contemporaneously with the onset of the clockwise rotation in Pacific-North America relative plate velocities (Atwater & Stock, 1998; Axen & Fletcher, 1998; Matti & Morton, 1993; Powell & Weldon, 1992). The timing of extension and plate boundary localization in Coachella Valley is synchronous with circa 6–8 Ma extension and subsequent plate boundary localization along the length of the Gulf of California rift (Bennett et al., 2013, 2016; Dorsey et al., 2011; Oskin & Stock, 2003; Pacheco et al., 2006; Seiler et al., 2011, 2013). Our AHe age results indicate that deformation in the northern Salton Trough was strongly partitioned between approximately E-W extension (e.g., on the WSDF) and N-W directed strike-slip faulting beginning with the inception of the transform plate boundary in the Salton Trough at circa 8 Ma. These results require reexamination of interpreted tectonic drivers related to an early (>12 Ma) inception of the WSDF ~30 km southwest of our study area (Shirvell et al., 2009).

Early Pleistocene to present tectonic reorganization and initiation of dextral strike-slip and normal faults along the western SRM represent a period of punctuated and high-rate uplift along a broad swath of the western part of the central Salton Block. High-angle normal faulting along the SRF and uplift along the western margin of the central Salton block elevated syntectonic and posttectonic strata on the east flank of the SRM

to ~1.4 km above sea level (Figure 7e) (Dorsey & Langenheim, 2015; Matti et al., 2002). The total magnitude of uplifted sedimentary deposits (~1.4 km) is identical to our estimate of vertical rock uplift in the southwest SRM since circa 1.2 Ma. Vertical deformation of the central Salton block is accommodated by the high-angle geometry of the SRF flower structure (Figure 7d). However, recent broad uplift of the SRM may be driven by oblique convergence along the SAF in Coachella Valley (Dorsey & Langenheim, 2015). Transpression and structural complexity within strands of the southern SAF zone are known to result in rapid vertical exhumation of spatially restricted crustal slivers (Spotila et al., 2001). Our results suggest that changes in local fault geometries (e.g., Fattaruso et al., 2014) can also affect far off-fault deformation across relatively large regions (hundreds of square kilometers) of transform plate boundaries.

6. Conclusions

New low-temperature thermochronometry (apatite U-Th/He; AHe) and thermal history modeling from the Santa Rosa Mountains (SRM), western Coachella Valley, constrain two late Miocene to present phases of extensional faulting. The first phase started at circa 8 Ma along the low-angle, east dipping West Salton Detachment Fault (WSDF)—a major regional fault within the southern San Andreas Fault (SAF) system—followed by a second phase that initiated at circa 1.2 Ma along the high-angle, southwest dipping Santa Rosa Fault (SRF), a splay within a negative flower structure associated with the San Jacinto Fault Zone (SJFZ). Elevation-age data from vertical transects of AHe samples from the eastern SRM support the presence of an exhumed Miocene helium partial retention zone, whereas samples from the SRF footwall in the southwest SRM represent a deeper crustal section, which cooled initially during down-to-the-east fault slip and footwall uplift of the WSDF then was fully exhumed during down-to-the-southwest slip on the high-angle SRF. The magnitude of vertical exhumation for the second phase is constrained by a regional tilt model informed by geometry of Miocene AHe isochrons in the SRM, geomorphology of the SRM, subsurface information from beneath Coachella Valley, and uplifted Neogene sediments along the eastern SRM. Pre-WSDF footwall paleodepths for structurally low samples from the SRF footwall were ~3.2 km depth at the onset of WSDF related exhumation. Vertical exhumation rates were likely between 0.15 and 0.36 km/Myr since WSDF initiation at circa 8 Ma until circa 1.2 Ma. WSDF slip rates were between ~1.2 and 3.0 km/Myr, based on the vertical component of exhumation and a fault dip of 7–15°. Total exhumation was temporally partitioned between this first low-angle detachment phase, followed by a second, high-angle phase along the SRF, responsible for ~1.4 km of vertical displacement at rates of ~1.3 km/Myr.

Initiation of the WSDF at circa 8 Ma supports a model in which plate boundary localization and formation of the southern SAF system in the Salton Trough were driven by the onset of an ~15–20° clockwise rotation of Pacific-North America relative plate velocities (Bennet & Oskin, 2014; Bennett et al., 2016). High-angle normal faulting and dextral strike-slip faulting associated with post-late 1.2 Ma transpression within the southern SAF system have partially overprinted the kinematics of the rifted western margin of the Salton Trough by dissecting the WSDF footwall and asymmetrically tilting the central Salton block down to the northeast. While low-temperature thermochronology has defined restricted, high-magnitude exhumation of crustal slivers between major strike-slip fault splays farther north along the SAF (e.g., Spotila et al., 2001), this study highlights the occurrence of punctuated, wide-spread, and relatively rapid vertical deformation of a crustal-scale block between the SAF zone and the SJFZ along the western margin of the Salton Trough. These results indicate that local fault geometry (e.g., Dorsey & Langenheim, 2015; Fattaruso et al., 2014; Fuis et al., 2012), and not plate motion obliquity to strike-slip faults (Teyssier, Tikoff, & Markley, 1995; Tikoff & Teyssier, 1994), may have exerted fundamental control on rock uplift rates during the evolution of the Pleistocene to recent southern SAF system.

Acknowledgments
Support for this study was provided by National Science Foundation grants EAR-1145115 (Spotila), EAR-0125307, EAR-0337775, and EAR-0809638 (Axen), and EAR-1144946 (Dorsey). Reviews from Anne Blythe, Scott Bennett, and feedback from the Associate Editor Michael Oskin significantly improved the scientific content and the style of this manuscript. C. M. acknowledges the Tectonics and Geomorphology Research Group and the Sedimentary Systems Research Group at Virginia Tech for constructive feedback. C. M. acknowledges Paul O'Sullivan for assistance with sample preparation. All sample locations, isotopic data, and resulting ages are available as supporting information in Table S1.

References

Atwater, T., & Stock, J. M. (1998). Pacific-North America plate tectonics of the Neogene southwestern United States: An update. *International Geology Review*, *40*(5), 375–402. https://doi.org/10.1080/00206819809465216

Axen, G. J. (1995). Extensional segmentation of the Main Gulf Escarpment, Mexico and United States. *Geology*, *23*(6), 515–518. https://doi.org/10.1130/009613(1995)023%3C0515:ESOTMG%3E2.3.CO;2

Axen, G. J. (1999). Low-angle normal fault earthquakes and triggering. *Geophysical Research Letters*, *26*(24), 3693–3696. https://doi.org/10.1029/1999GL005405

Axen, G. J., & Fletcher, J. M. (1998). Late Miocene-Pleistocene extensional faulting, northern Gulf of California, Mexico and Salton Trough, California. *International Geology Review*, *40*(3), 217–244. https://doi.org/10.1080/00206819809465207

Axen, G. J., Grove, M., Stockli, D., Lovera, O. M., Rothstein, D. A., Fletcher, J. M., … Abbott, P. L. (2000). Thermal evolution of Monte Blanco dome: Low-angle normal faulting during Gulf of California rifting and late Eocene denudation of the eastern Peninsular Ranges. *Tectonics*, *19*(2), 197–212. https://doi.org/10.1029/1999TC001123

Behr, W. M., Rood, D. H., Fletcher, K. E., Guzman, N., Finkel, R., Hanks, T. C., … Yule, J. D. (2010). Uncertainties in slip-rate estimates for the Mission Creek strand of the southern San Andreas Fault at Biskra Palms Oasis, southern California. *Bulletin Geological Society of America*, *122*, 1360–1377. https://doi.org/10.1130/B30020.1

Bennet, S. E. K., & Oskin, M. E. (2014). Oblique rifting ruptures continents: Example from the Gulf of California shear zone. *Geology*, *42*(3), 215–218. https://doi.org/10.1130/G34904.1

Bennett, S. E. K., Oskin, M. E., & Iriondo, A. (2013). Transtensional rifting in the proto-Gulf of California, near Bahía Kino, Sonora, México. *Geological Society of America Bulletin*, *125*(11-12), 1752–1782. https://doi.org/10.1130/B30676.1.

Bennett, S. E. K., Oskin, M. E., Dorsey, R. J., Iriondo, A., & Kunk, M. J. (2015). Stratigraphy and structural development of the southwest Isla Tiburón marine basin: Implications for latest Miocene tectonic opening and flooding of the northern Gulf of California. *Geosphere*, *11*(4), 977–1007. https://doi.org/10.1130/GES01153.1

Bennett, S. E. K., Oskin, M. E., Iriondo, A., & Kunk, M. J. (2016). Slip history of the La Cruz fault: Development of a late Miocene transform in response to increased rift obliquity in the northern Gulf of California. *Tectonophysics*, *693*, 409–435. https://doi.org/10.1016/j.tecto.2016.06.013

Brown, R. W., Beucher, R., Roper, S., Persano, C., Stuart, F., & Fitzgerald, P. (2013). Natural age dispersion arising from the analysis of broken crystals. Part I: Theoretical basis and implications for the apatite (U–Th)/He thermochronometers. *Geochimica et Cosmochimica Acta*, *122*, 478–497. https://doi.org/10.1016/j.gca.2013.05.041

Buscher, J. T., & Spotila, J. A. (2007). Near-field response to transpression along the southern San Andreas fault, based on exhumation of the northern San Gabriel Mountains, southern California. *Tectonics*, *26*, TC5004. https://doi.org/10.1029/2006TC002017

Cox, B. F., Matti, J. C., King, T., & Morton, D. M. (2002). Neogene strata of southern Santa Rosa Mountains, California, and their significance for tectonic evolution of the western Salton Trough. *Geological Society of America Abstracts with Programs*, *34*(6), 57–55.

Crowell, J. C. (1981). An outline of the tectonic history of southeastern California. In W. G. Ernst (Ed.), *The geotectonic development of California; Rubey*, *Englewood Cliffs* (Vol. I, pp. 583–600). NJ: Prentice-Hall.

Darin, M. H., Bennett, S. E. K., Dorsey, R. J., Oskin, M. E., & Iriondo, A. (2016). Late Miocene extension in coastal Sonora, México: Implications for the evolution of dextral shear in the proto-Gulf of California oblique rift. *Tectonophysics*, *693*, 378–408. https://doi.org/10.1016/j.tecto.2016.04.038

dePolo, C. M., & Anderson, J. G. (2000). Estimating the slip rates of normal faults in the Great Basin, USA. *Basin Research*, *12*(3-4), 227–240. https://doi.org/10.1046/j.1365-2117.2000.00131.x

Dibblee, T. W. Jr. (1954). Geology of the Imperial Valley region, California. In R. H. Jahns (Ed.), *Geology of Southern California* (Vol. 170, pp. 21–28). California Division of Mines Bulletin.

Dibblee, T. W. (1984). Stratigraphy and tectonics of the San Felipe Hills, Borrego Badlands, Superstition Hills, and vicinity. In C. A. Rigsby (Ed.), *The Imperial Basin—Tectonics, sedimentation, and thermal aspects*, *Soc. of Econ. Paleontol. And Mineral* (pp. 31–44). Los Angeles, CA: Pacific Section.

Dodson, M. H. (1973). Closure temperature in cooling geochronological and petrological systems. *Contributions to Mineralogy and Petrology*, *40*(3), 259–274. https://doi.org/10.1007/BF00373790

Dorsey, R. J. (2002). Stratigraphic record of Pleistocene initiation and slip on the Coyote Creek fault, lower Coyote Creek, southern California, in Barth, a., ed., contributions to crustal evolution of the southwest United States. *Geological Society of America Special Papers*, *365*, 251–269. https://doi.org/10.1130/0-8137-2365-5.251

Dorsey, R. J., & Langenheim, V. E. (2015). Crustal-scale tilting of the central Salton block, southern California. *Geosphere*, *11*(5), 1365–1383. https://doi.org/10.1130/GES01167.1

Dorsey, R. J., & Lazear, G. (2013). A post–6 Ma sediment budget for the Colorado River. *Geosphere*, *9*(4), 781–791. https://doi.org/10.1130/GES00784.1

Dorsey, R. J., & Roering, J. J. (2006). Quaternary landscape evolution in the San Jacinto fault zone, Peninsular Ranges of Southern California: Transient response to strike-slip fault initiation. *Geomorphology*, *73*, 16–32. https://doi.org/10.1016/j.geomorphology,2005.06.013

Dorsey, R. J., Housen, B. A., Janecke, S. U., Fanning, C. M., & Spears, A. L. F. (2011). Stratigraphic record of basin development within the San Andreas fault system: Late Cenozoic fish Creek-Vallecito basin, Southern California. *Bulletin Geological Society of America*, *123*, 771–793. https://doi.org/10.1130/B30168.1

Dorsey, R. J., Axen, G. J., Peryam, T. C., & Kairouz, M. E. (2012). Initiation of the Southern Elsinore Fault at ~1.2 Ma: Evidence from the Fish Creek-Vallecito Basin, southern California. *Tectonics*, *31*, TC2006. https://doi.org/10.1029/2011TC003009

Dumitru, T. A. (1990). Subnormal Cenozoic geothermal gradients in the extinct Sierra Nevada magmatic arc: Consequences of Laramide and post-Laramide shallow-angle subduction. *Journal of Geophysical Research*, *95*(B4), 4925–4941. https://doi.org/10.1029/JB095iB04p04925

Ehlers, T. A., & Farley, K. A. (2003). Apatite (U–Th)/He thermochronometry: Methods and applications to problems in tectonic and surface processes. *Earth and Planetary Science Letters*, *206*(1-2), 1–14. https://doi.org/10.1016/S0012-821X(02)01069-5

Ehlig, P. L. (1981). Origin and tectonic history of the basement terrane of the San Gabriel Mountains, central transverse ranges. In W. G. Ernst (Ed.), *The geotectonic development of California; Rubey*, *Englewood Cliffs* (Vol. I, pp. 253–283). NJ: Prentice-Hall.

Farley, K. A. (2000). Helium diffusion from apatite: General behavior as illustrated by Durango fluorapatite. *Journal of Geophysical Research*, *105*(B2), 2903–2914. https://doi.org/10.1029/1999JB900348

Farley, K. A., & Stockli, D. F. (2002). (U-Th)/He dating of phosphates: Apatite, monazite, and xenotime. In M. J. Kohn, J. Rakovan, & J. M. Hughes (Eds.), *Phosphates: Geochemical, geobiological, and materials importance*, *Rev. Mineral. Geochem* (Vol. 48, pp. 559–577). Washington, DC: Mineralogical Society of America.

Farley, K. A., Wolf, R. A., & Silver, L. T. (1996). The effects of long a-stopping distances on (U-Th)/He ages. *Geochimica et Cosmochimica Acta*, *60*(21), 4223–4229. https://doi.org/10.1016/S0016-7037(96)00193-7

Fattaruso, L. a., Cooke, M. L., & Dorsey, R. J. (2014). Sensitivity of uplift patterns to dip of the San Andreas Fault in the Coachella Valley, California. *Geosphere*, *10*(6), 1235–1246. https://doi.org/10.1130/GES01050.1

Flowers, R. M., Ketcham, R. A., Shuster, D. L., & Farley, K. A. (2009). Apatite (U–Th)/He thermochronometry using a radiation damage accumulation and annealing model. *Geochimica et Cosmochimica Acta*, *73*, 2347–2365. https://doi.org/10.1016/j.gca.2009.01.015

Fuis, G. S., Scheirer, D. S., Langenheim, V. E., & Kohler, M. D. (2012). A new perspective on the geometry of the San Andreas Fault in southern California and its relationship to lithospheric structure. *Seismological Society of America Bulletin*, *102*, 236–251. https://doi.org/10.1785/0120110041

Gallagher, K. (2012). Transdimensional inverse thermal history modeling for quantitative thermochronology. *Journal of Geophysical Research*, *117*, B02408. https://doi.org/10.1029/2011JB008825

Grove, M., Lovera, O., & Harrison, M. (2003). Late Cretaceous cooling of the east-central Peninsula Ranges batholith (33°N): Relationship to La Posta pluton emplacement, Laramide shallow subduction, and forearc sedimentation. In S. E. Johnson, et al. (Eds.), *Tectonic evolution of northwestern Mexico and the southwestern USA*. *Geological Society of America Special Paper*, *374*, 355–379. https://doi.org/10.1130/0-8137-2374-4.355

Herbert, J. W., & Cooke, M. L. (2012). Sensitivity of the southern San Andreas fault system to tectonic boundary conditions and fault configurations. *Seismological Society of America Bulletin*, *102*, 2046–2062. https://doi.org/10.1785/0120110316

Ingersoll, R. V., & Rumelhart, P. E. (1999). Three-stage evolution of the Los Angeles basin. *Southern California: Geology*, *27*(7), 593–596. https://doi.org/10.1130/0091-7613(1999)027%3C0593:TSEOTL%3E2.3.CO;2

Janecke, S. U., Dorsey, R. J., Steely, A. N., Kirby, S. M., Lutz, A. T., Housen, B. A., … Forand, D. (2010). High geologic slip rates since early Pleistocene initiation of the San Jacinto and San Felipe fault zones in the San Andreas fault system: Southern California, USA. *Geological Society of America Special Papers*, *475*, 48. https://doi.org/10.1130/9780813724751

Ketcham, R. A. (2005). Forward and inverse modeling of low-temperature thermochronometry data. *Reviews in Mineralogy and Geochemistry*, *58*, 275–314. https://doi.org/10.2138/rmg.2005.58.11

King, T., Cox, B. F., Matti, J. C., Powell, C. L., Osterman, L. E., & Bybell, L. M. (2002). Previously unreported outcrops of Neogene Imperial Formation in southern Santa Rosa Mountains, California, and implications for tectonic uplift. *Geological Society of America Abstracts with Programs*, *34*(6), 57–56.

Kirby, S. M., Janecke, S. U., Dorsey, R. J., Housen, B. A., Langenheim, V., McDougall, K., & Steely, A. N. (2007). Pleistocene Brawley and Ocotillo formations: Evidence for initial strike-slip deformation along the San Felipe and San Jacinto fault zones, southern California. *Journal of Geology*, *115*, 43–62. https://doi.org/10.1086/509248

Langenheim, V. E., Jachens, R. C., Matti, J. C., Hauksson, E., Morton, D. M., & Christensen, A. (2005). Geophysical evidence for wedging in the San Gorgonio Pass structural knot, southern San Andreas Fault zone, southern California-marked. *Geological Society of America Bulletin*, *117*(11), 1554. https://doi.org/10.1130/B25760.1

Lin, G. (2013). Three-dimensional seismic velocity structure and precise earthquake relocations in the Salton Trough, Southern California. *Bulletin of the Seismological Society of America*, *103*(5), 2694–2708. https://doi.org/10.1785/0120120286

Lin, G., Shearer, P. M., & Hauksson, E. (2007). Applying a three-dimensional velocity model, waveform cross correlation, and cluster analysis to locate southern California seismicity from 1981 to 2005. *Journal of Geophysical Research*, *112*, B12309. https://doi.org/10.1029/2007JB004986

Lindsey, E. O., & Fialko, Y. (2013). Geodetic slip rates in the southern San Andreas fault system: Effects of elastic heterogeneity and fault geometry. *Journal of Geophysical Research: Solid Earth*, *118*, 689–697. https://doi.org/10.1029/2012JB009358

Loveless, J. P., & Meade, B. J. (2011). Stress modulation on the San Andreas Fault by interseismic fault system interactions. *Geology*, *39*, 1035–1038. https://doi.org/10.1130/G32215.1

Luo, G., & Liu, M. (2012). Multi-timescale mechanical coupling between the San Jacinto Fault and the San Andreas Fault, southern California. *Lithosphere*, *4*, 221–229. https://doi.org/10.1130/L180.1

Lutz, A. T., Dorsey, R. J., Housen, B. A., & Janecke, S. U. (2006). Stratigraphic record of Pleistocene faulting and basin evolution in the Borrego Badlands, San Jacinto fault zone, Southern California. *Geological Society of America Bulletin*, *118*, 1377–1397. https://doi.org/10.1130/B25946.1

Matti, J. C., & Morton, D. M. (1993). Paleogeographic evolution of the San Andreas Fault in southern California: A reconstruction based on a new cross-fault correlation. In R. E. Powell, et al. (Eds.), *The San Andreas Fault System: Displacement, palinspastic reconstruction, and geologic evolution*. *Geological Society of America Memoir*, *178*, 107–159. https://doi.org/10.1130/MEM178-p107

Matti, J. C., Cox, B. F., Morton, D. M., Sharp, R. V., & King, T. (2002). Fault-bounded Neogene sedimentary deposits in the Santa Rosa Mountains, southern California: Crustal stretching or transpressional uplift? *Geological Society of America Abstracts with Programs*, *34*(6), 57–54.

Matti, J. C., Morton, D. M., Cox, B. F., Landis, G. P., Langenheim, V. E., Premo, W. R., … Budahn, J. R. (2006). Fault-bounded late Neogene sedimentary deposits in the Santa Rosa Mountains, southern CA: Constraints on the evolution of the San Jacinto fault. *Eos, Transactions of the American Geophysical Union*, *87*, T21B–0407.

Meade, B. J., & Hager, B. H. (2005). Block models of crustal motion in southern California constrained by GPS measurements. *Journal of Geophysical Research*, *110*, B03403. https://doi.org/10.1029/2004JB003209

Morton, D. M., & Matti, J. C. (1993). Extension and contraction within an evolving divergent strike-slip fault complex: The San Andreas and San Jacinto fault zones at their convergence in Southern California. *Geological Society of America Memoir*, *178*, 217–230. https://doi.org/10.1130/MEM178-p217

Nicholson, C., Sorlien, C. C., Atwater, T., Crowell, J. C., & Luyendyk, B. P. (1994). Microplate capture, rotation of the western transverse ranges, and initiation of the San Andreas transform as a low-angle fault system. *Geology*, *22*(6), 491–495. https://doi.org/10.1130/0091-613%5B1994%5D022%3C0491:MCROTW%3E2.3.CO;2

Nicholson, C., Plesch, A., Shaw, J., Sorlein, C., & Hauksson, E. (2013). Updating the 3D fault set for the SCEC Community Fault Model (CFM-v4) and revising its associated fault database [poster]: Southern California earthquake center annual meeting.

Oskin, M., & Stock, J. (2003). Pacific-North America plate motion and opening of the upper Delfin Basin, northern Gulf of California, Mexico. *Geological Society of America Bulletin*, *115*(10), 1173–1190. https://doi.org/10.1130/B25154.1

Pacheco, M., Martín-Barajas, A., Elders, W., Espinosa-Cardena, J. M., Helenes, J., & Segura, A. (2006). Stratigraphy and structure of the Altar basin of NW Sonora: Implications for the history of the Colorado River delta and the Salton Trough. *Revista Mexicana de Ciencias Geology*, *23*, 22.

Powell, R. E. (1981). Geology of the crystalline basement complex, eastern transverse ranges, southern California: Constraints on regional tectonic interpretation, dissertation (PhD dissertation). California Institute of Technology. http://resolver.caltech.edu/CaltechETD:etd-07252007-135803

Powell, R. E., & Weldon, R. J. II (1992). Evolution of the San Andreas Fault. *Annual Review of Earth and Planetary Sciences*, *20*(1), 431–468. https://doi.org/10.1146/annurev.ea.20.050192.002243

Roeske, S. M., Till, A. B., Foster, D. A., & Sample, J. C. (2007). Introduction. In A. B. Till, et al. (Eds.), *Exhumation associated with continental strike-slip fault systems*. *Geological Society of America Special Paper*, *434*, vii–vix. https://doi.org/10.1130/978-0-8137-2434-8(2007)434%5Bvii:I%5D2.0.CO;2

Seiler, C., Fletcher, J. M., Kohn, B. P., Gleadow, A. J. W., & Raza, A. (2011). Low-temperature thermochronology of northern Baja California, Mexico: Decoupled slip-exhumation gradients and delayed onset of oblique rifting across the Gulf of California. *Tectonics*, *30*, TC3004. https://doi.org/10.1029/2009TC002649

Seiler, C., Quigley, M. C., Fletcher, J. M., Phillips, D., Gleadow, A. J. W., & Kohn, B. P. (2013). Stratigraphy and $^{40}Ar/^{39}Ar$ geochronology of the Santa Rosa basin, Baja California: Dynamic evolution of a constrictional rift basin during oblique extension in the Gulf of California. *Basin Research*, *25*(4), 388–418. https://doi.org/10.1111/bre.12004

Sharp, R. V. (1967). San Jacinto fault zone in the Peninsular Ranges of southern California. *Geological Society of America Bulletin*, *78*(6), 705–730. https://doi.org/10.1130/0016-7606(1967)78%5B705:SJFZIT%5D2.0.CO;2

Shirvell, C. R., Stockli, D. F., Axen, G. J., & Grove, M. (2009). Miocene–Pliocene exhumation along the west Salton detachment fault, southern California, from (U-Th)/He thermochronometry of apatite and zircon. *Tectonics*, *28*, TC2006. https://doi.org/10.1029/2007TC002172

Shuster, D. L., Flowers, R. M., & Farley, K. A. (2006). The influence of natural radiation damage on helium diffusion kinetics in apatite. *Earth and Planetary Science Letters*, *249*, 148–161. https://doi.org/10.1016/j.epsl.2006.07.028

Simpson, C. (1984). Borrego Springs-Santa Rosa mylonite zone: A Late Cretaceous west-directed thrust in southern California. *Geology*, *12*(1), 8–11. https://doi.org/10.1130/0091-7613(1984)12%3C8:BSRMZA%3E2.0.CO;2

Smith-Konter, B., & Sandwell, D. T. (2009). Stress evolution of the San Andreas fault system: Recurrence interval versus locking depth. *Geophysical Research Letters*, *36*, L13304. https://doi.org/10.1029/2009GL037235

Spencer, J. E., & Normark, W. R. (1979). Tosco-Abreojos fault zone: A Neogene transform plate boundary within the Pacific margin of southern Baja California, Mexico. *Geology*, *7*(11), 554–557. https://doi.org/10.1130/0091-7613%5B1979%5D7%3C554:TFZANT%3E2.0.CO;2

Spotila, J. A. (2005). Applications of low-temperature thermochronometry to tectonic geomorphology, based on examples from transpressional and convergent settings, in Reiners, P.W., ed., low temperature thermochronometry: Techniques, interpretations, and applications, reviews in mineralogy and geochemistry. *Mineralogical Society American*, *58*, 449–466.

Spotila, J. A., & Berger, A. L. (2010). Exhumation at orogenic indentor corners under long-term glacial conditions: Example of the St. Elias orogen, Southern Alaska. *Tectonophysics*, *490*, 241–256. https://doi.org/10.1016/j.tecto.2010.05.015

Spotila, J. A., & Sieh, K. (2000). Architecture of transpressional thrust faulting in the San Bernardino Mountains, southern California, from deformation of a deeply weathered surface. *Tectonics*, *19*(4), 589–615. https://doi.org/10.1029/1999TC001150

Spotila, J. A., Farley, K. A., & Sieh, K. (1998). Uplift and erosion of the San Bernardino Mountains, associated with transpression along the San Andreas Fault, CA, as constrained by radiogenic helium thermochronometry. *Tectonics*, *17*(3), 360–378. https://doi.org/10.1029/98TC00378

Spotila, J. A., Farley, K. A., Yule, J. D., & Reiners, P. (2001). Near-field transpressive deformation along the San Andreas fault zone in southern California, based on exhumation constrained by (U-Th)/He dating. *Journal of Geophysical Research*, *106*(B12), 30,909–30,922. https://doi.org/10.1029/2001JB000348

Spotila, J. A., Niemi, N. A., Brady, R. C., House, M. A., Buscher, J. T., & Oskin, M. (2007). Long-term continental deformation associated with transpressive plate motion: The San Andreas Fault. *Geology*, *35*, 967–970. https://doi.org/10.1130/G23816A.1

Steely, A. N., Janecke, S. U., Dorsey, R. J., & Axen, G. J. (2009). Early Pleistocene initiation of the San Felipe fault zone, SW Salton Trough, during reorganization of the San Andreas fault system. *Geological Society of America Bulletin*, *121*, 663–687. https://doi.org/10.1130/B26239.1

Stock, J. M., & Hodges, K. V. (1989). Pre-Pliocene extension around the Gulf of California and the transfer of Baja California to the Pacific Plate. *Tectonics*, *8*(1), 99–115. https://doi.org/10.1029/TC008i001p00099

Stockli, D. F. (2005). Application of low-temperature thermochronometry to extensional settings, in low- temperature thermochronology: Techniques, interpretations, and applications, edited by P. W. Reiners & T. A. Ehlers. *Reviews in Mineralogy and Geochemistry*, *58*, 411–448. https://doi.org/10.2138/rmg.2005.58.16

Teyssier, C., Tikoff, B., & Markley, M. (1995). Oblique plate motion and continental tectonics. *Geology*, *23*(5), 447–450. https://doi.org/10.1130/0091-7613(1995)023%3C0447:OPMACT%3E2.3.CO;2

Thatcher, W., Savage, J. C., & Simpson, R. W. (2016). The Eastern California Shear Zone as the northward extension of the southern San Andreas fault. *Journal of Geophysical Research: Solid Earth*, *121*, 2904–2914. https://doi.org/10.1002/2015JB012678

Tikoff, B., & Teyssier, C. (1994). Strain modelling of displacement-field partitioning in transpressional orogens. *Journal of Structural Geology*, *16*(11), 1575–1588. https://doi.org/10.1016/0191-8141(94)90034-5

Todd, V. R., Erskine, B. G., & Morton, D. M. (1988). Metamorphic and tectonic evolution of the northern Peninsular Ranges Batholith, southern California. In W. G. Ernst (Ed.), *Metamorphism and crustal evolution of the Western United States: Rubey Volume VII. Englewood Cliffs* (pp. 894–937). NJ: Prentice-Hall.

U.S. Geological Survey (and California Geological Survey) (2006). Quaternary fault and fold database for the United States, accessed November 2015, from USGS web site: http//earthquakes.usgs.gov/hazards/qfaults/

Wernicke, B. (1985). Uniform-sense normal simple shear of the continental lithosphere. *Canadian Journal of Earth Sciences*, *22*(1), 108–125. https://doi.org/10.1139/e85-009

Wolf, R. A., Farley, K. A., & Silver, L. T. (1996). Helium diffusion and low-temperature thermochronometry of apatite. *Geochimica et Cosmochimica Acta*, *60*(21), 4231–4240. https://doi.org/10.1016/S0016-7037(96)00192-5

Wolf, R. A., Farley, K. A., & Silver, L. T. (1997). Assessment of (U-Th)/He thermochronometry: The low-temperature history of the San Jacinto Mountains, California. *Geology*, *25*(1), 65–68. https://doi.org/10.1130/0091-7613(1997)025%3C0065:AOUTHT%3E2.3.CO;2

Wolf, R. A., Farley, K. A., & Kass, D. M. (1998). Modeling of the temperature sensitivity of the apatite (U-Th)/He thermochronometer. *Chemical Geology*, *148*(1-2), 105–114. https://doi.org/10.1016/S0009541(98)00024-2